### Geometric Priors for Generalizable World Models via Vector Symbolic Architecture

Editors: List of editors' names

### Abstract

A key challenge in artificial intelligence and neuroscience is understanding how neural systems learn representations that capture the underlying dynamics of the world. Most world models represent the transition function with unstructured neural networks, limiting interpretability, sample efficiency, and generalization to unseen states or action compositions. We address these issues with a generalizable world model grounded in Vector Symbolic Architecture (VSA) principles as geometric priors. Our approach utilizes learnable Fourier Holographic Reduced Representation (FHRR) encoders to map states and actions into a high-dimensional complex vector space with learned group structure and models transitions with element-wise complex multiplication. We formalize the framework's group-theoretic foundation and show how training such structured representations to be approximately invariant enables strong multi-step composition directly in latent space and generalization performances over various experiments. On a discrete grid world environment, our model achieves 87.5% zero-shot accuracy to unseen state-action pairs, obtains 53.6% higher accuracy on 20-timestep horizon rollouts, and demonstrates  $4\times$  higher robustness to noise relative to an MLP baseline. These results highlight how training to have latent group structure yields generalizable, data-efficient, and interpretable world models, providing a principled pathway toward structured models for real-world planning and reasoning.

**Keywords:** World Models, Vector Symbolic Architecture, Hyperdimensional Computing, Fourier Holographic Reduced Representation, Neurosymbolic AI, Geometric Deep Learning

### 1. Introduction

Humans build internal world models that capture the underlying dynamics of the environment and allow interaction beyond direct trial-and-error (LeCun, 2022). Inspired by this idea, modern reinforcement learning (RL) has leveraged latent predictive models conditioned on states and actions, achieving state-of-the-art results in video games (Hafner et al., 2020) and continuous control (Hansen et al., 2023). Despite these successes, current world models face two major limitations. They are largely confined to RL, control, and robotics settings where abundant simulated data is available and treat the transition function  $T: S \times A \to S$  as an **unstructured** black-box function approximator realized by neural networks that lack any built-in geometric priors. While highly expressive, such architectures suffer from poor sample efficiency, weak extrapolation to unseen states, compounding rollout errors, and latent spaces with no explicit geometric meaning.

Biological systems, in contrast, appear to exploit symmetries and geometric structure (Gardner et al., 2022; Gallego et al., 2017) in the environment, effectively reducing the complexity of learning. Geometric Deep Learning (GDL) (Bronstein et al., 2021; Papillon et al., 2025; Shewmake et al., 2023) formalizes this idea by incorporating geometric priors into neural networks to help preserve structure throughout the network, dramatically improving the efficiency and generalization capabilities.

Vector Symbolic Architecture (VSA) (Kleyko et al., 2022) offers a complementary, algebraic approach to structured representations. They represent symbols as high-dimensional vectors and compose them via binary operations, forming structured representations that are robust to noise. In addition, VSA-based representations can be trained to approximate group actions, making them a promising approach for GDL. Among the many VSA variants, Fourier Holographic Reduced Representation (FHRR) (Plate, 2003) remains a popular implementation of VSA to efficiently encode complex data structures due to its efficiency and exact invertibility.

Contribution. In this work, we propose a generalizable world model using VSA principles. Our FHRR encoder encodes states and actions as unitary complex vectors, with transitions realized as element-wise multiplication. We train the model to have latent group structure on actions with multi-step action composition, invertibility, and robust cleanup. We demonstrate that the model (1) encourages transition equivariance in the latent space and learns action representations respecting group structure, (2) achieves long-horizon stability and error correction via cleanup, and (3) outperforms MLP baselines on one-step prediction, long-horizon rollouts, zero-shot generalization, and robustness tests on a discrete grid world environment regardless of scale. Our approach provides an alternative architecture to world modeling with strong implications for interpretable and generalizable decision-making for real world applications.

### 2. Related Work

World Models in Model-Based RL. World models aim to learn a predictive model of an environment's transition dynamics that can leveraged for learning and planning. Model-based reinforcement learning methods (Ha and Schmidhuber, 2018; Hafner et al., 2019) and recent Model Predictive Control methods (Hansen et al., 2023) utilize world models to learn the environment's dynamics for decision-making, yet often suffer from compounding rollout errors (Hansen et al., 2022) and limited transparency in the learned dynamics (Glanois et al., 2024). Most approaches treat the transition function as an unstructured mapping from  $(s, a) \mapsto s'$ , which can be highly expressive but fails to exploit known symmetries in the environment. This can limit generalization, especially when the environment exhibits strong symmetries or if little training data is available. These limitations motivate the incorporation of geometric priors into world models, where known symmetries or structures in the environment are part of the representation learning process.

Geometric Deep Learning. In the context of world modeling, GDL-based approaches (Kipf et al., 2019; Park et al., 2022) have incorporated symmetry and structure to improve generalization in structured environments. However, in such implementations, the group action is enforced through the transition model's architecture, and the latent representations themselves are not structured such that they can be algebraically composed, inverted, or directly manipulated. Without the ability to easily or interpretably manipulate latents with vector operations, planning or composition with such architectures consequently require an expensive full forward pass or additionally trained modules. Our VSA-based approach to GDL trains the action representations such that it respects group structure in the latent space and leverages cleanup for robustness and compounding error reduction.

Vector Symbolic Architectures. VSA, also known as Hyperdimensional Computing, is a computational paradigm where discrete symbols are represented as high-dimensional vectors (e.g.  $D \geq 1000$ ) sampled from well-defined distributions (Kanerva, 2009). These distributed representations are inherently robust to noise and enable symbolic reasoning through algebraic operations on vectors. VSAs have been applied in diverse domains, including efficient classification (Hernández-Cano et al., 2021; Ni et al., 2024b), time-series modeling (Mejri et al., 2024), graph reasoning (Poduval et al., 2022), reinforcement learning (Ni et al., 2024a), and representing cognitive maps (Yeung et al., 2025). Hardware-efficient implementations have also made them appealing for resource-constrained applications and learning on the edge (Zou et al., 2021; Chung et al., 2025). While VSA has been applied to various domains, its applications as a transition operation in learnable settings remain largely unexplored. Our work aims to close this gap by constructing learnable world models that utilize the binding operation to model environment transitions and the VSA clean-up mechanism to perform robust rollouts.

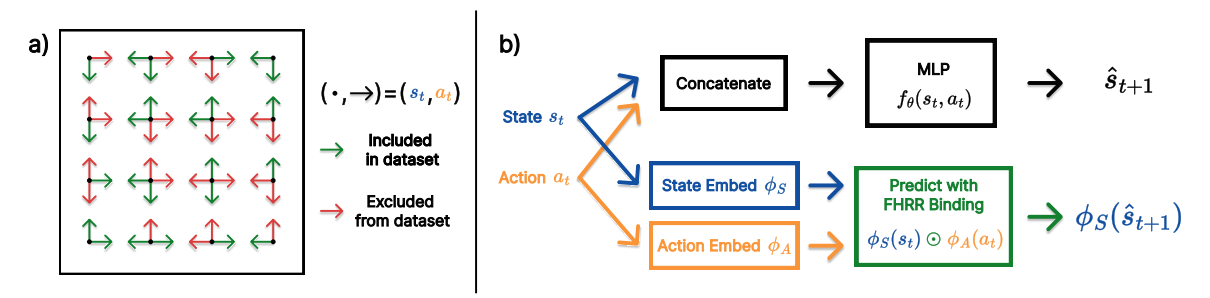


Figure 1: Overview of the FHRR-based world modeling framework. a) Visualization of the partially held-out GridWorld Environment. b) Difference between MLP-based and FHRR-based dynamics modeling. Direct predictions of  $\hat{s}_{t+1}$  by MLPs cannot easily generalize to OOD samples, while FHRR can.

### 3. Proposed Framework

Figure 1 visualizes the architecture of our generalizable world model. We model environment dynamics as group actions in a learnable, complex latent space where the dynamics is implemented by the binding operation. Concretely, we learn state and action encoders such that the transition model inherits several useful VSA properties including interpretability of the transformation between two given states, robustness to noise due to the high-dimensionality of the representations, and a native cleanup mechanism to mitigate exponential error growth in long-horizon rollouts. In contrast, MLP-based approaches take the concatenation of state-action pairs which limits the model's ability to learn separate state and action mappings. In this section, we introduce the mathematical formulation that allows the model to generalize.

### 3.1. Fourier Holographic Reduced Representation

FHRR (Plate, 2003) is a specific VSA variant in which each vector component lies on the unit circle in the complex plane, i.e.

$$\mathbf{v} = [e^{i\theta_j}]_{j=1}^D \in \mathbb{C}^D \tag{1}$$

such that  $\theta_j \sim p$  for dimension  $j=1,\ldots,D$  where p is some distribution (e.g. Unif $(0,2\pi)$  or  $\mathcal{N}(0,1)$ ), resulting in a phase-based complex unitary vector. As a VSA, FHRR admits binary operations, namely bundling (+) and binding  $(\odot)$ , to construct composite representations. Bundling is implemented as vector addition while binding is implemented as element-wise complex multiplication. Given vectors  $\mathbf{v}_1 = [e^{i\theta_{1,j}}]_{j=1}^D$  and  $\mathbf{v}_2 = [e^{i\theta_{2,j}}]_{j=1}^D$ ,  $\mathbf{v}_1 \odot \mathbf{v}_2 = [e^{i(\theta_{1,j}+\theta_{2,j})}]_{j=1}^D$ . The inverse of a FHRR vector  $\mathbf{v}$  is simply its complex conjugate, enabling straightforward unbinding via  $\mathbf{v}^{-1} = \overline{\mathbf{v}}$ . FHRR is the extension of Holographic Reduced Representations, which consists of real-valued components and circular convolution as binding (Appendix A). FHRR avoids convolution and fourier transforms altogether by using element-wise complex multiplication which is equivalent to convolution in the frequency domain (Plate, 2003). A notable property of FHRR is its connection to kernel-based methods in machine learning (Appendix A.2). There are various other related implementations of VSA (Appendix A), but we limit the scope of VSA to FHRR in this work.

### 3.2. Environment Dynamics as a Group Action on Sets

Let S be a finite set of states, A a finite set of actions, and  $T: S \times A \to S$  a deterministic transition function. We assume that compositions of actions generate an action group  $(G, \circ)$  acting on S:

$$\cdot: G \times S \to S, \quad (g, s) \mapsto g \cdot s,$$
 (2)

with identity  $e \cdot s = s$  and  $(g_1 \circ g_2) \cdot s = g_1 \cdot (g_2 \cdot s)$  for  $g_1, g_2 \in G$ . Each action  $a \in A$  corresponds to a generator  $g_a \in G$  such that  $T(s, a) = g_a \cdot s$ . In particular, the identity e does not need to be a primitive action, but is always present in G and can be realized as  $e = g_a \circ g_a^{-1}$  for any  $a \in A$ .

**Example:** (10×10 GridWorld) Let  $S = \mathbb{Z}_{10} \times \mathbb{Z}_{10}$ , and let  $G = \mathbb{Z}_{10} \times \mathbb{Z}_{10}$  act by translations. The four actions correspond to the generators (±1,0) and (0,±1) (i.e., *left*, *right*, *up*, and *down*). With wrap-around, G is abelian while without wrap-around, the action structure is a local group with boundary effects and  $S = [10] \times [10]$  where  $[n] = \{1, 2, ..., n\}$ .

### 3.3. Equivariant Latent Representations

We embed states into a D-dimensional complex vector space via a map  $\phi_S: S \to \mathcal{Z}$ , where  $\mathcal{Z} = (S^1)^D = \{z \in \mathbb{C}^D : |z_d| = 1\}$ . Notably,  $(\mathcal{Z}, \odot)$  forms a group. A representation of the action group G in  $\mathcal{Z}$  is a homomorphism

$$\rho: G \to \mathcal{Z}, \quad \rho(g_1 \circ g_2) = \rho(g_1) \odot \rho(g_2), \quad \forall g_1, g_2 \in G.$$
 (3)

The encoder  $\phi_S: S \to \mathcal{Z}$  is equivariant to environment transitions if

$$\phi_S(T(s,a)) = \rho(a) \odot \phi_S(s), \quad \forall s \in S, \ a \in A$$
 (4)

where T(s, a) is the environment's transition function. By closure of G, the same property holds for any composed action  $g \in G$ , i.e.  $\phi_S(g \cdot s) = \rho(g) \odot \phi_S(s)$ , which states that transforming s by g corresponds to multiplying its latent representation by  $\rho(g)$ .

### 3.4. Latent Transition Model

We would like to learn state and action encoders,  $\phi_S: S \to \mathcal{Z}$  and  $\phi_A: A \to \mathcal{Z}$  respectively, such that (1)  $\phi_A$  induces a representation of G via the generators  $g_a \in G$  for all  $a \in A$ ; and (2) the equivariance condition given by Eq. 4 holds.

Suppose  $s \in \mathbb{R}^{n_s}$  and  $a \in \mathbb{R}^{n_a}$  where  $n_s$  and  $n_a$  are the state and action dimensions, respectively. We parametermize  $\phi_S$  and  $\phi_A$  via the FHRR encoding

$$\phi_S(s) = [e^{i\theta_{j,s}^{\top}s}]_{j=1}^D, \quad \phi_A(a) = [e^{i\theta_{j,a}^{\top}a}]_{j=1}^D$$
 (5)

Motivated by Eq. 4, we model the latent transitions in FHRR-space via the binding operator

$$\tau: \mathcal{Z} \times \mathcal{Z} \to \mathcal{Z}, \quad (\phi_S(s), \phi_A(a)) \mapsto \phi_S(s) \odot \phi_A(a)$$
 (6)

We would also like to learn  $\phi_S: S \to \mathcal{Z}$  and  $\phi_A: A \to \mathcal{Z}$  such that one-step dynamics satisfy

$$\phi_S(s_{t+1}) = \tau(\phi_S(s_t), \phi_A(a_t)) = \phi_S(s_t) \odot \phi_A(a_t), \tag{7}$$

and  $\phi_A(a) = \rho(g_a)$ . In phase coordinates, this corresponds to:

$$\Theta_s^{\top} s_{t+1} = \Theta_s^{\top} s_t + \Theta_a^{\top} a_t \pmod{2\pi}$$
 (8)

where  $\Theta_s = [\theta_{j,s}]_{j=1}^D \in \mathbb{C}^{D \times n_s}$ ,  $\Theta_a = [\theta_{j,a}]_{j=1}^D \in \mathbb{C}^{D \times n_a}$ , and the modulus is applied elementwise. Due to the properties of FHRR, we can simply extend this to multi-step composition:

Embedding Space: 
$$\phi_S(s_{t+k}) = \phi_S(s_t) \odot \prod_{j=1}^k \phi_A(a_{t+j-1})$$
 (9)

Phase Space: 
$$\Theta_s^{\top} s_{t+k} = \Theta_s^{\top} s_t + \sum_{j=1}^k \Theta_a^{\top} a_{t+j-1} \pmod{2\pi}.$$
 (10)

### 3.5. Learning Objectives

We learn  $\phi_S$  and  $\phi_A$  with learnable parameters  $\Theta_s$  and  $\Theta_a$  respectively and train on transition tuples,  $(s_t, a_t, s_{t+1})$ . We minimize a binding loss to encourage transition equivariance given in Eq. 7:

$$\mathcal{L}_{\text{bind}} = \|\phi_S(s_{t+1}) - \phi_S(s_t) \odot \phi_A(a_t)\|^2$$
(11)

Additionally, to preserve structure in our representations, we introduce invertibility and orthogonality regularizers:

$$\mathcal{L}_{\text{inv}} = \sum_{(a, a^{-1})} \| \phi_A(a) \odot \phi_A(a^{-1}) - \mathbf{1} \|^2,$$
 (12)

$$\mathcal{L}_{\text{ortho}} = \sum_{i \neq j} \left( \langle \phi_S(s_i), \phi_S(s_j) \rangle \right)^2. \tag{13}$$

In particular, the invertability constraint given by Eq. 12 encourages that the actions  $a \in A$  form a representation via  $\phi_A$ , i.e.  $\phi_A$  induces an approximate homomorphism with respect to the actions in the grid environment.

The full objective is  $\mathcal{L} = \lambda_{\text{bind}} \mathcal{L}_{\text{bind}} + \lambda_{\text{inv}} \mathcal{L}_{\text{inv}} + \lambda_{\text{ortho}} \mathcal{L}_{\text{ortho}}$  where  $\lambda_{\text{bind}}$ ,  $\lambda_{\text{inv}}$ ,  $\lambda_{\text{ortho}}$  are the hyperparameters controlling the balance between each objective respectively. Training is linear-time in D per sample and memory is O(D) as all VSA operations are done elementwise. Additionally, multi-step rollouts can be processed using Eq. 10 for linear-time in the phase space where  $(|a| \in A) \ll D$  for inference.

### 3.6. Cleanup Mechanism

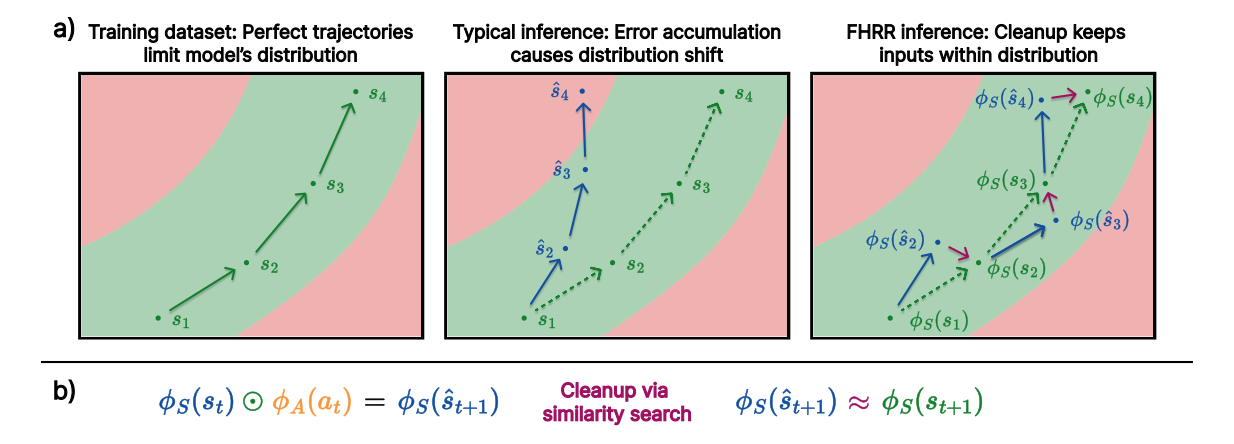


Figure 2: a) Shaded red represents out of the training distribution. Cleanup during FHRR Inference can ameliorate error accumulation due to distribution shift between train and test. b) Cleanup mechanism equations via similarity search in FHRR.

A key advantage of VSA-based models is their ability to support error correction through a process known as *cleanup*, shown in Figure 2. In our setting, each state  $s \in S$  is encoded as a unitary complex vector, and during training the  $\mathcal{L}_{ortho}$  term (Section 3.5) enforces that distinct state representations are *quasi-orthogonal*, i.e. Re  $\langle \phi_S(s), \phi_S(s') \rangle \approx 0$  for  $s \neq s'$ .

As D increases, the capacity to maintain larger separation margins between symbols improves, which directly enhances cleanup robustness. Given a noisy or approximate prediction of the next-state,  $\phi_S(\hat{s}_{t+1})$ , cleanup recovers the most likely true embedding by similarity search, i.e.  $\phi_S(\hat{s}_{t+1}) = \arg\max_{s \in \mathcal{S}} \operatorname{Re} \langle \phi_S(\hat{s}_{t+1}), \phi_S(s) \rangle$ . When the state-codebook is explicitly stored as a matrix, this operation can be reduced to taking an arg max after performing matrix-vector multiplication.

### 4. Results

**Experimental Design.** We train and evaluate 2 variants of VSA-based world models and 3 MLP baselines of varying sizes on a  $10\times10$  GridWorld environment with a total of 100 discrete states and 4 deterministic actions. For all models, we train on 80% of (state, action) pairs, hold out 20% for zero-shot evaluation, and train for 500 epochs. For our VSA-based models we use embedding dimensions of D = 512 while for MLP we use D = 64, D = 16 for state and action which are concatenated and a hidden dimension of D = 128. In Table 4, we compare Holographic Reduced Representations (HRR) and FHRR

# Proceedings Track

Table 1: VSA-Based vs MLP Dynamics Modeling

Task	VSA (HRR)	VSA (FHRR)	MLP-S	MLP-M	MLP-L
1-step Accuracy	91.0%	$\boldsymbol{96.3\%}$	80.0%	80.0%	80.25%
1-step Accuracy (Zero-Shot)	80.0%	87.5%	0.0%	0.0%	1.25%
Cosine Similarity	82.5	83.0	79.5	79.9	80.6
Cosine Similarity (Zero-Shot)	71.1	80.5	0.9	0.15	3.1
Rollout (5 steps)	70.8%	$\boldsymbol{74.6\%}$	39.8%	38.0%	40.8%
Rollout (20 steps)	3.2%	<b>34.6</b> %	2.0%	4.0%	6.2%
Rollout (20 steps $+$ Clean)	45.4%	$\boldsymbol{61.4\%}$	5.4%	7.8%	8.4%
Rollout (100 steps)	0.6%	1.8%	0.8%	1.8%	<b>2.0</b> %
Rollout (100 steps $+$ Clean)	6%	$\boldsymbol{38.6\%}$	2.8%	4.0%	3.2%

versus MLP-Small, MLP-Medium, and MLP-Large on several different tasks, such as 1-step accuracy, cosine similarity, and rollouts. In Appendix B.5, we compare the total parameter count and inference time between all the models to highlight that VSA models have a similar parameter count as MLP-S (MLP-S is  $0.8\times$ , MLP-M is  $4.5\times$ , MLP-L is  $26.2\times$  the parameter count as VSA models). For more explicit details on the implementation, please check the Appendix B.

**Dynamics Modeling** For 1-step accuracy, we test the models on their ability to predict the correct next state given (state, action) pairs. While the models are trained on 80% of the dataset, they are tested on all possible transitions. VSA-FHRR achieves a higher 1-step prediction accuracy than all the MLP variations and also outperforms VSA-HRR (realvalued, binding through circular convolution). The 1-step accuracy of all MLP variations are seemingly limited by the amount of data they train on at 80%. For the zero-shot tests (when evaluating on the unseen 20% transitions), VSA-based models achieves significantly higher zero-shot accuracy and cosine similarity, confirming its ability to generalize well. We also highlight that scaling the size of the MLPs has not shown a stronger ability for these models to generalize. In the rollout tests, we compare VSA and MLP methods on their latent rollout accuracy when predicting over long horizons (i.e. interactions solely in the latent space without receiving a state from the environment). FHRR maintains a higher accuracy over long transitions, unlike MLP which accumulates drift. Additionally, VSA has the added benefit of applying *cleanup*. For a fair comparison, we utilize nearestneighbor search for the MLPs to compare against the VSA models with cleanup and apply the cleanup every 2 time steps.

Latent Rollout Performance. Figure 3 compares the latent rollout accuracy of horizon length t=20 between FHRR and MLP-M given varying zero-shot ratios. As the zero-shot ratio increases, we notice a linear decrease in the FHRR model performance while the MLP-based model's accuracy exponentially decreases and fails to maintain even above 10% when trained on only 90% of the transitions. Additionally, the cleanup operation improves the accuracy of the FHRR model by 35% when zero-shot ratio = 0.1, resulting in a  $3.3\times$  improvement over the MLP baseline. As expected, we also emphasize that the cleanup

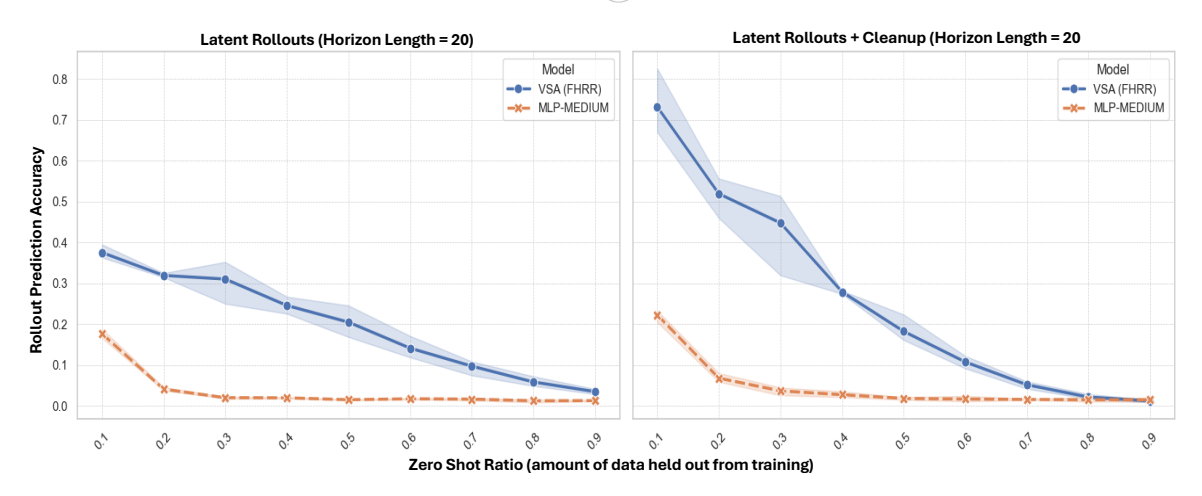


Figure 3: Latent Rollout Accuracy of FHRR and MLP-M over varying zero-shot ratios

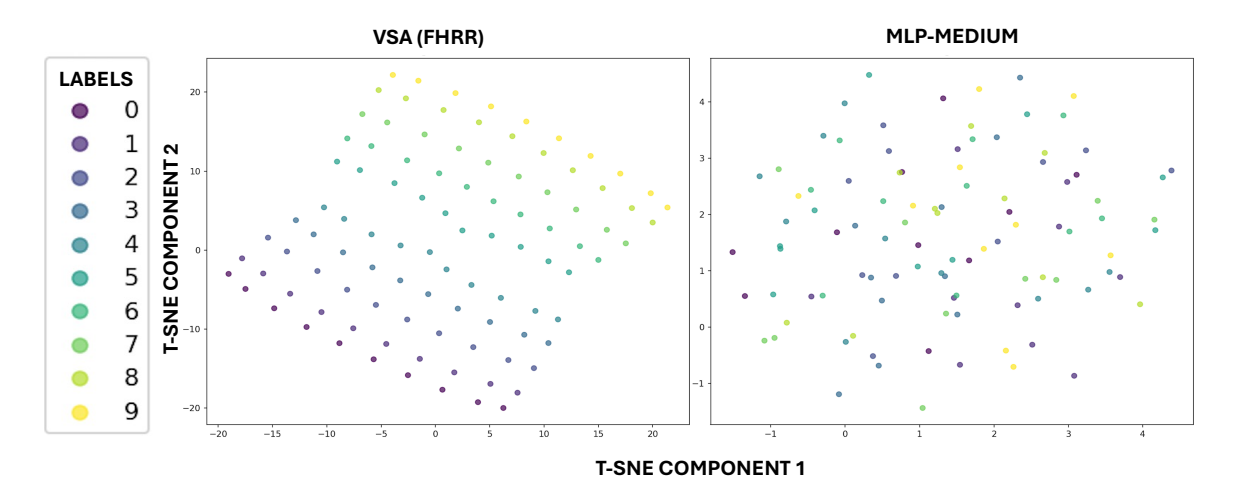


Figure 4: t-SNE visualization of state embeddings for VSA (FHRR) vs MLP-M labeled per row

operation has little to no benefit for the MLP-based model due to the lack of structure and quasi-orthogonality.

Latent Visualizations. In Figure 4 we visualize the t-SNE components of the state embeddings of the VSA-FHRR and MLP-Medium models. The VSA-FHRR model is able to capture the structure of the grid environment in its latent space while MLP-Medium fails to maintain any structure. We attribute this structured latent space for its strong generalization capabilities over MLP baselines.

**Robustness.** We study the robustness of our FHRR model with MLP-M by comparing the 1-step dynamics accuracy when random gaussian noise is added to the transition function. Figure 5(a) shows the results between gaussian noise between 0 to 5 magnitude of standard deviation (i.e. noise  $n \sim \mathcal{N}(0, \sigma)$  where  $\sigma \in [0, 5]$ ). The FHRR model maintains

# Proceedings Track

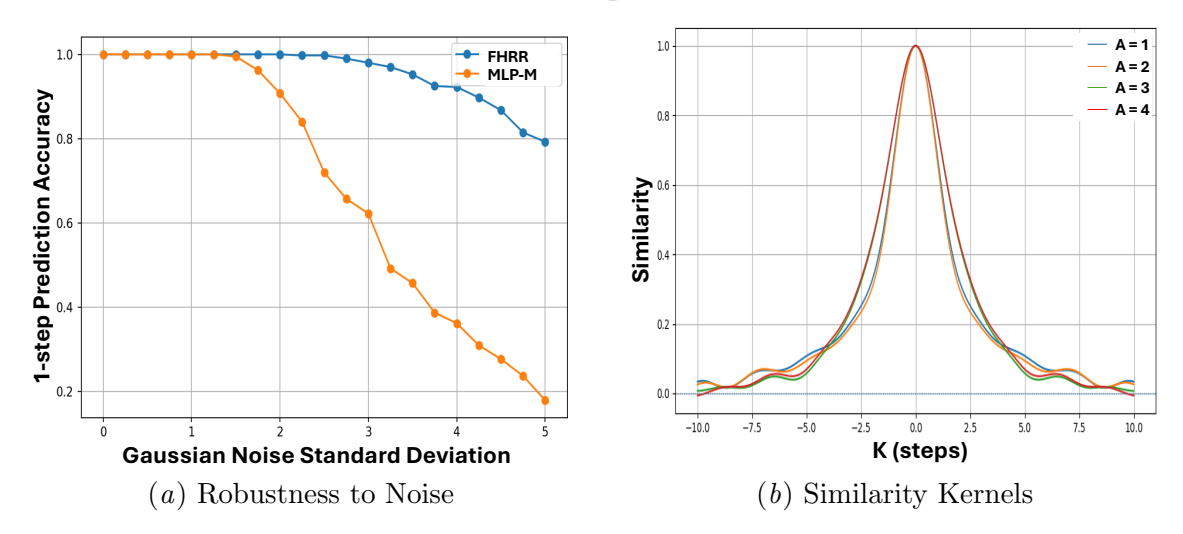


Figure 5: VSA (FHRR) vs MLP-Medium on robustness and similarity experiments

above a 80% accuracy even under large amounts of noise while MLP-M struggles as the scale of noise increases. Specifically, the FHRR model has above  $4\times$  higher prediction accuracy than MLP-M under noisy conditions.

Similarity Kernel. Given the kernel approximation property of FHRR (Appendix A.2), in Figure 5(b), we plot the similarity between  $\phi_S(s)$  and  $\phi_S(s+ka)$  where a is a given action and  $k \in [-10, 10]$ . For all actions, we notice an approximately smooth but sharp similarity kernel peaking at k = 0 and decaying as |k| increases, indicating that the latent space preserves locality of the states. States that can be reached by 1 or 2 actions are closer in similarity while further ones become nearly orthogonal (e.g. similarity  $\approx 0$ ). The approximate symmetry of these curves across actions demonstrates that our model learns a structured geometry in which actions correspond to consistent translation across the states.

### 5. Conclusion

In this work, we present an alternative approach to world modeling based on VSA, where states and actions are encoded as unitary complex vectors and transitions are modeled via element-wise multiplication. Our experiments on a discrete world environment show that our model achieves strong generalization capabilities and maintains long-horizon rollout accuracy under noise, outperforming MLP baselines regardless of scale. While promising, our current work is limited to small discrete environments. Extending this approach to continuous, stochastic, or partially observable domains remains an open challenge. In future work, we hope to integrate VSA-based world modeling into model-based RL and planning to enable generalizable dynamics models that are applicable to real world environments. Overall, this work demonstrates that learning structured algebraic representations offers a principled path toward robust, interpretable, and generalizable world models.

### References

- Michael M Bronstein, Joan Bruna, Taco Cohen, and Petar Veličković. Geometric deep learning: Grids, groups, graphs, geodesics, and gauges. arXiv preprint arXiv:2104.13478, 2021.
- William Youngwoo Chung, Hamza Errahmouni Barkam, Tamoghno Das, and Mohsen Imani. Robust reasoning and learning with brain-inspired representations under hardware-induced nonlinearities. In *Proceedings of the Great Lakes Symposium on VLSI 2025*, pages 968–975, 2025.
- Juan A Gallego, Matthew G Perich, Lee E Miller, and Sara A Solla. Neural manifolds for the control of movement. *Neuron*, 94(5):978–984, 2017.
- Richard J Gardner, Erik Hermansen, Marius Pachitariu, Yoram Burak, Nils A Baas, Benjamin A Dunn, May-Britt Moser, and Edvard I Moser. Toroidal topology of population activity in grid cells. *Nature*, 602(7895):123–128, 2022.
- Ross W. Gayler. Multiplicative Binding, Representation Operators & Analogy. 1998. URL https://www.semanticscholar.org/paper/Multiplicative-Binding%2C-Representation-Operators-%26-Gayler/94ee052b3016fe1967699714ab0eb8d4bfeca26e.
- Claire Glanois, Paul Weng, Matthieu Zimmer, Dong Li, Tianpei Yang, Jianye Hao, and Wulong Liu. A survey on interpretable reinforcement learning. *Machine Learning*, 113 (8):5847–5890, 2024.
- David Ha and Jürgen Schmidhuber. World models. arXiv preprint arXiv:1803.10122, 2018.
- Danijar Hafner, Timothy Lillicrap, Jimmy Ba, and Mohammad Norouzi. Dream to control: Learning behaviors by latent imagination. arXiv preprint arXiv:1912.01603, 2019.
- Danijar Hafner, Timothy Lillicrap, Mohammad Norouzi, and Jimmy Ba. Mastering atari with discrete world models. arXiv preprint arXiv:2010.02193, 2020.
- Nicklas Hansen, Xiaolong Wang, and Hao Su. Temporal difference learning for model predictive control. arXiv preprint arXiv:2203.04955, 2022.
- Nicklas Hansen, Hao Su, and Xiaolong Wang. Td-mpc2: Scalable, robust world models for continuous control. arXiv preprint arXiv:2310.16828, 2023.
- Alejandro Hernández-Cano, Namiko Matsumoto, Eric Ping, and Mohsen Imani. Onlinehd: Robust, efficient, and single-pass online learning using hyperdimensional system. In 2021 Design, Automation & Test in Europe Conference & Exhibition (DATE), pages 56–61. IEEE, 2021.
- Pentti Kanerva. Hyperdimensional computing: An introduction to computing in distributed representation with high-dimensional random vectors. *Cognitive computation*, 1:139–159, 2009.

### Proceedings Track

- Thomas Kipf, Elise Van der Pol, and Max Welling. Contrastive learning of structured world models. arXiv preprint arXiv:1911.12247, 2019.
- Denis Kleyko, Dmitri A Rachkovskij, Evgeny Osipov, and Abbas Rahimi. A survey on hyperdimensional computing aka vector symbolic architectures, part i: Models and data transformations. *ACM Computing Surveys*, 55(6):1–40, 2022.
- Yann LeCun. A path towards autonomous machine intelligence version 0.9. 2, 2022-06-27. Open Review, 62(1):1-62, 2022.
- Mohamed Mejri, Chandramouli Amarnath, and Abhijit Chatterjee. A novel hyperdimensional computing framework for online time series forecasting on the edge. arXiv preprint arXiv:2402.01999, 2024.
- Yang Ni, William Y Chung, Samuel Cho, Zhuowen Zou, and Mohsen Imani. Efficient exploration in edge-friendly hyperdimensional reinforcement learning. In *Proceedings of the Great Lakes Symposium on VLSI 2024*, pages 111–118, 2024a.
- Yang Ni, Zhuowen Zou, Wenjun Huang, Hanning Chen, William Youngwoo Chung, Samuel Cho, Ranganath Krishnan, Pietro Mercati, and Mohsen Imani. Heal: Brain-inspired hyperdimensional efficient active learning. arXiv preprint arXiv:2402.11223, 2024b.
- Mathilde Papillon, Sophia Sanborn, Johan Mathe, Louisa Cornelis, Abby Bertics, Domas Buracas, Hansen J Lillemark, Christian Shewmake, Fatih Dinc, Xavier Pennec, and Nina Miolane. Beyond euclid: an illustrated guide to modern machine learning with geometric, topological, and algebraic structures. *Machine Learning: Science and Technology*, 6(3): 031002, August 2025. ISSN 2632-2153. doi: 10.1088/2632-2153/adf375. URL http://dx.doi.org/10.1088/2632-2153/adf375.
- Jung Yeon Park, Ondrej Biza, Linfeng Zhao, Jan Willem van de Meent, and Robin Walters. Learning symmetric embeddings for equivariant world models. arXiv preprint arXiv:2204.11371, 2022.
- Tony A Plate. Holographic reduced representations. *IEEE Transactions on Neural networks*, 6(3):623–641, 1995.
- Tony A Plate. Holographic Reduced Representation: Distributed representation for cognitive structures, volume 150. CSLI Publications Stanford, 2003.
- Prathyush Poduval, Haleh Alimohamadi, Ali Zakeri, Farhad Imani, M Hassan Najafi, Tony Givargis, and Mohsen Imani. Graphd: Graph-based hyperdimensional memorization for brain-like cognitive learning. *Frontiers in Neuroscience*, 16:757125, 2022.
- Ali Rahimi and Benjamin Recht. Random features for large-scale kernel machines. In J. Platt, D. Koller, Y. Singer, and S. Roweis, editors, *Advances in Neural Information Processing Systems*, 2007.
- Christian Shewmake, Domas Buracas, Hansen Lillemark, Jinho Shin, Erik Bekkers, Nina Miolane, and Bruno Olshausen. Visual scene representation with hierarchical equivariant sparse coding. 2023. URL https://par.nsf.gov/biblio/10529135.

- Calvin Yeung, Zhuowen Zou, and Mohsen Imani. Generalized Holographic Reduced Representations, 2024. URL http://arxiv.org/abs/2405.09689.
- Calvin Yeung, Zhuowen Zou, Nathaniel D. Bastian, and Mohsen Imani. Cognitive map formation under uncertainty via local prediction learning. 27:200551, 2025. ISSN 2667-3053. doi: 10.1016/j.iswa.2025.200551. URL https://www.sciencedirect.com/science/article/pii/S2667305325000778.
- Zhuowen Zou, Haleh Alimohamadi, Farhad Imani, Yeseong Kim, and Mohsen Imani. Spiking hyperdimensional network: Neuromorphic models integrated with memory-inspired framework. arXiv preprint arXiv:2110.00214, 2021.

## Proceedings Track

### Appendix A. Vector Symbolic Architectures

### A.1. VSA Variants

VSA consists of two fundamental operations: **bundling** (superposition), which adds vectors to form set-like representations, and **binding** (association), which combines vectors into a compositional representation, often with invertibility. This algebraic structure allows VSAs to represent structured data such as sequences, sets, and relations in a way that supports compositionality and symbolic reasoning through lightweight vector operations.

Many VSA works also consist of a **permutation** operation (shuffling) to encode ordered structures or design non-commutative operations when combined with **bundling** or **binding**. Below, we summarize some related VSA approaches:

Holographic Reduced Representations HRR (Plate, 1995) uses real-valued vectors with components drawn from a normal distribution and defines binding as circular convolution, bundling as element-wise addition, and similarity as dot product between two vectors.

Multiply Add Permute MAP (Gayler, 1998) utilizes high-dimensional bipolar vectors where binding is element-wise multiplication, bundling is element-wise addition, and similarity as cosine similarity or the dot product. MAP forms the foundation for many subsequent VSA designs due to the simplicity of element-wise multiplication for binding.

Generalized Holographic Reduced Representations GHRR (Yeung et al., 2024) is an extension of FHRR by replacing the unitary complex vector  $e^{i\theta} \in U(1)$  with a unitary matrix  $a_j \in U(m)$ , such that vectors become tensors  $H \in \mathbb{C}^{D \times m \times m}$  whose binding is defined as matrix multiplication. Bundling still holds as element-wise addition. The similarity between two hypervectors  $H_1 = [a_j]_{j=1}^D$  and  $H_2 = [b_j]_{j=1}^D$  is defined as

$$\delta(H_1, H_2) = \frac{1}{mD} \operatorname{Re} \left( \operatorname{tr} \sum_{j=1}^{D} a_j b_j^{\dagger} \right). \tag{14}$$

For m=1, this reduces exactly to FHRR similarity. GHRR enables non-commutative and more flexible representations, controlled by the choice of unitary matrices yet equivalent to FHRR when m=1.

### A.2. Kernel Approximation in FHRR

One way to encode data into FHRR follows the Random Fourier Features (RFF) encoding (Rahimi and Recht, 2007), an efficient approximation of kernel methods. The RFF encoding is a map  $\phi : \mathbb{R}^n \to \mathbb{C}^D$ , with  $\phi(\mathbf{x}) = e^{i\mathbf{M}\mathbf{x}}$ , where each row  $\mathbf{M}_{j,:} \sim p$  for some multivariate distribution p. As a result of Bochner's theorem,  $\langle \phi(\mathbf{x}), \phi(\mathbf{y}) \rangle / D \approx K(\mathbf{x} - \mathbf{y})$  for all  $\mathbf{x}, \mathbf{y} \in \mathbb{R}^n$ , where K is a shift-invariant kernel that is the Fourier transform of distribution p. The approximation converges to the true kernel in the limit as  $D \to \infty$ . Notably, when p is the standard Gaussian distribution, the radial basis function (RBF) kernel is recovered.

### Appendix B. Implementation Details

#### **B.1.** Environment

**Dataset** We use a  $10 \times 10$  GridWorld with boundaries (no wrap-around). States are indexed and mapped to (row, col). Actions  $a \in \{0, 1, 2, 3\}$  correspond to up, down, left, right with deterministic transition T(s, a) = (s').

We define transitions (s, a, s') for  $s \in S$ ,  $a \in A$ , which yields  $|S||A| = 100 \times 4$  tuples. We form a zero-shot split at the level of given a zero-shot ratio, such that a fixed ratio (default 20%) of pairs (s, a) are withheld from training. Zero-shot evaluations are done only held-out pairs, while the regular accuracy, cosine similarity, rollout tests are all done with the all the transitions.

### **B.2.** Models

Our VSA-based models use embedding dimensions of D=512. HRR initializes its weights as real-valued numbers sampled from a normal distribution with mean =0 and standard deviation =1. We utilize circular convolution for the binding and circular correlation for unbinding. For FHRR, we sample the elements from a uniform distribution from -pi to pi and utilize element-wise complex multiplication for binding. For MLP-based models, we use D=64 and D=16 for the state and action respectively. These state and actions are concatenated and fed into a MLP for next state prediction. MLP-S is constructed with 2 hidden layer (D=128), MLP-M with 4 hidden layers (D=256), and MLP-L with 6 hidden layers (D=512). Every hidden layer's output passes through a ReLU activation as well.

### **B.3.** Training Objectives and Hyperparameters

For both VSA and MLP-based models. we utilize MSE for the binding loss in 11. For all experiments, the binding  $\lambda_{\rm bind}=2$ ,  $\lambda_{\rm inv}=0.5$ , and  $\lambda_{\rm ortho}=0.05$ . The learning rate for VSA models is set as 0.007 where as the learning rate for MLP-based models is set as 0.0005. We apply a gradient clipping of 1 to help with learning as well.

### **B.4.** Experiments

All experiments were run conducted over 500 epochs. For the rollout tests, we sample 500 trials of random trajectories based on the horizon length (i.e. Rollout Length = 20 implies a random trajectory with t=20). We apply the cleanup operation to both VSA and MLP-based models every 2 time steps when specified as rollout + cleanup.

In Figure 6 we run an ablation study and see that increasing dimensionality helps with robustness as expected. Having an orthogality weight is also necessary but shows little benefit of increasing the weight itself. On the other hand, increasing the number of parameters hurts the robustness of an MLP-based model.

#### **B.5.** Inference Details

In Table B.5, we display the number of parameters of each model as well as the inference time. Experiments were conducted using an NVIDIA GPU 3060 Ti and inference times were reported in milliseconds.

# Proceedings Track



Figure 6: Robustness Ablation Study

Table 2: VSA vs MLP Parameter and Inference Speed

	VSA (HRR)	VSA (FHRR)	MLP-S	MLP-M	MLP-L
Parameter Count	53,248	53,248	41,600	241,024	1,394,048
Parameter Ratio	1x	1x	0.8x	4.5x	26.2x
Inference time (ms)	0.2063	0.1528	0.1174	0.1715	0.3135
Inference + Clean time (ms)	0.2632	0.2421	0.1743	0.2317	0.3761

### B.6. Cleanup

Because unrelated vectors are nearly orthogonal, small perturbations to  $\hat{s}_{t+1}$  do not change the identity of the nearest neighbor, ensuring correct retrieval. By contrast, conventional neural networks often learn latent spaces without explicit separation or compositional structure. In such unstructured spaces, small prediction errors can change the nearest neighbor in latent space, leading to semantic drift that compounds over long roll-outs and even incompatibility with inherently noisy emerging hardware alternatives (e.g. processing in-memory and neuromorphic computing). Given a perturbed output  $\hat{s}_{t+1} = f_{\theta}(s, a) + \epsilon$ , it is not guaranteed that:

$$\arg\min_{s'} \|f_{\theta}(s, a) - \hat{s}_{t+1}\| \approx s_{t+1}.$$

Nearest-neighbor search in such spaces is unreliable and semantically ambiguous, as it does not preserve identity or symbolic structure. When the number of states is manageable (e.g. discrete environments), this allows error correction at each timestep with negligible overhead, maintaining prediction accuracy and stability even over long horizons. In practice, when  $|\mathcal{S}|$  is large, batch-restricted cleanup or approximate nearest neighbor can be used to speed up the process.

In practice, the similarity metric often used for cleanup in FHRR is the real part of the cosine similarity between two vectors, Re  $\langle \phi_S(s), \phi_S(s') \rangle$ .